Chinese Chemical Letters 32 (2021) 1372–1376

Contents lists available at ScienceDirect

Chinese Chemical Letters

journal homepage: www.elsevier.com/locate/cclet

Communication

Solution-processed multi-resonance organic light-emitting diodes with high efficiency and narrowband emission

Shen Xu[a,b], Qingqing Yang[a], Ying Zhang[a], Hui Li[a], Qin Xue[c], Guohua Xie[c,*], Minzhao Gu[a], Jibiao Jin[a], Ling Huang[b,*], Runfeng Chen[a,*]

[a] Key Laboratory for Organic Electronics and Information Displays & Jiangsu Key Laboratory for Biosensors, Institute of Advanced Materials (IAM), Jiangsu National Synergistic Innovation Center for Advanced Materials (SICAM), Nanjing University of Posts & Telecommunications, Nanjing 210023, China
[b] Key Laboratory of Flexible Electronics (KLOFE) & Institute of Advanced Materials (IAM), Nanjing Tech University, Nanjing 211816, China
[c] Sauvage Center for Molecular Sciences, Hubei Key Lab on Organic and Polymeric Optoelectronic Materials, Department of Chemistry, Wuhan University, Wuhan 430072, China

ARTICLE INFO

Article history:
Received 22 July 2020
Received in revised form 15 October 2020
Accepted 19 October 2020
Available online 22 October 2020

Keywords:
Multi-resonance
Thermally activated delayed fluorescence
Solution-processed devices
Charge-transfer delocalization
Narrowband emission

ABSTRACT

With excellent color purity (full-width half maximum (FWHM) < 40 nm) and high quantum yield, multi-resonance (MR) molecules can harvest both singlet and triplet excitons for highly efficient narrowband organic light-emitting diodes (OLEDs) owing to their thermally activated delayed fluorescence (TADF) nature. However, the highly rigid molecular skeleton with the oppositely positioned boron and nitrogen in generating MR effects results in the intrinsic difficulties in the solution-processing of MR-OLEDs. Here, we demonstrate a facile strategy to increase the solubility, enhance the efficiencies and modulate emission color of MR-TADF molecules by extending aromatic rings and introducing *tert*-butyls into the MR backbone. Two MR-TADF emitters with smaller singlet-triplet splitting energies (ΔE_{ST}) and larger oscillator strengths were prepared conveniently, and the solution-processed MR-OLEDs were fabricated for the first time, exhibiting efficient bluish-green electroluminescence with narrow FWHM of 32 nm and external quantum efficiency of 16.3%, which are even comparable to the state-of-the-art performances of the vacuum-evaporated devices. These results prove the feasibility of designing efficient solution-processible MR molecules, offering important clues in developing high-performance solution-processed MR-OLEDs with high efficiency and color purity.

Thermally activated delayed fluorescence (TADF) emitters, which can realize 100% internal quantum efficiency through efficient reverse intersystem crossing (RISC) of triplet excitons without the involvement of any rare noble metals, have drawn tremendous attention especially in the field of organic light-emitting diodes (OLEDs) [1–3]. Plenty of TADF materials have been developed since the pioneering work of Adachi *et al.* [4,5], showing the increasingly improved external quantum efficiencies (EQEs) even higher than those of phosphorescent OLEDs [6,7]. To design efficient TADF emitters, strong electron donor (D) and acceptor (A) units are generally incorporated in D-A architectures to spatially separate the highest occupied molecular orbital (HOMO) and the lowest unoccupied molecular orbital (LUMO) and consequently minimized the splitting energy (ΔE_{ST}) between the lowest singlet (S_1) and triplet (T_1) excited states, because a small ΔE_{ST} (< 0.37 eV) is essential in supporting efficient RISC process at room temperature [8–10]. Nevertheless, these D-A molecules with strong intramolecular charge transfer (ICT) characters often display fairly small radiative emission cross-sections and are usually accompanied by large structural reorganization related to high conformational degrees of freedom of the D-A molecular architecture [11]. Therefore, the emission spectra of most TADF emitters are considerably broad with full-width half maximum (FWHM) close to 100 nm without fine structures, leading to poor color purity of the TADF OLEDs which is fatal for active matrix displays.

Alternatively, Hatakeyama et al. proposed an unusual design strategy of TADF molecules by introducing nitrogen and boron atoms positioned oppositely in a rigid polycyclic aromatic framework to induce the multi-resonance (MR) effects; an atomically separated distribution of HOMO and LUMO for small ΔE_{ST} and relatively large oscillator strength (f_{osc}) are resulted, where HOMO locates on nitrogen atoms and carbon atoms at the *meta* positions of nitrogen atoms, and LUMO distributes mainly on

* Corresponding authors.
E-mail addresses: guohua.xie@whu.edu.cn (G. Xie), iamlhuang@njtech.edu.cn (L. Huang), iamrfchen@njupt.edu.cn (R. Chen).

https://doi.org/10.1016/j.cclet.2020.10.022

boron atoms and carbon atoms at the *meta* positions of boron atoms [12,13]. This localization of HOMO and LUMO induced by MR effects minimizes the bonding/antibonding character, vibronic coupling and vibrational relaxation in the material, resulting in an extremely sharp photoluminescence (PL) spectrum with a very small FWHM and significantly reduced ΔE_{ST} to promote RISC for efficient TADF emission with large f_{osc} [14,15]. Many high-performance MR-type blue TADF molecules have been developed, showing high EQEs up to 34.4% and narrow emission bands with FWHM of 14 nm [16,17]. In contrast, narrowband green and red MR-TADF emitters are fairly rare owing to the intrinsic difficulties in bathochromic shift of the MR-featured emission. Effective ways reported to improve the luminescent efficiencies and manipulate the emission colors of MR-TADF materials include increasing the number of MR backbones in either linear or cyclic molecular structures and introducing various substituents on the MR systems to amplify the influence of skeleton and peripheral units [18,19]. Nevertheless, along with the much increased synthetic difficulties and preparation costs, the resulting MR-TADF molecules generally exhibit reduced solubility due to the increased molecular rigidity and planarity [20]. Therefore, the most reported MR-TADF-based OLEDs were fabricated by vacuum deposition and the solution-processed MR-OLEDs remain a challenge so far [21,22].

Here, we demonstrate that both the emission color and efficiency of MR-TADF molecules can be modulated by introducing additional aromatic rings into the MR backbone (Fig. 1). Owing to the expanded conjugation skeleton and increased molecular planarity, the facilely prepared MR-TADF emitter of **CzBN** shows sky-blue emission with a small ΔE_{ST} of 0.12 eV and a large oscillator strength of 0.3506. The first fabricated solution-processed MR-OLEDs exhibit high device performance with EQE up to 14.7% and FWHM of 35 nm. To further bathochromic shift the emission band and improve the solubility, *tert*-butyls were introduced at the *para* positions of nitrogen atoms. Excitingly, thus designed MR molecule of **BCzBN** has bluish-green emission around 490 nm with PLQY of 86% and FWHM of 32 nm, and the solution-processed TADF devices reach the high EQEs up to 16.3%. This combined aromatization and substitution strategy of the MR skeleton not only provides an effective way to design high-performance MR-TADF materials, but also makes the solution-processed MR-OLEDs possible.

Based on the widely investigated deep-blue MR-TADF emitter of **DABNA-1** [12], the two free-rotating peripheral benzenes of nitrogen atoms were designed to be fused to their nearby benzene rings in the core to afford **CzBN**. This aromatization of the skeleton not only extends the π-conjugation but also increases the ICT localization area for the more efficient MR effect [14]. To increase the solubility and further modulate emission band, four electron-donating *tert*-butyl substituents were introduced to the *para* positions of the two nitrogen atoms to obtain **BCzBN**. These molecules can be facilely prepared by replacing diphenylamine to carbazole in a similar two-step synthetic route of **DABNA-1** with total yields up to 36% (Scheme S1 in Supporting information). The molecular structures were fully characterized by ^{1}H and ^{13}C NMR (Figs. S1-S6 in Supporting information) [23]. Extraordinarily, they have good solubility in comment solvents, which is up to 10 mg/mL for **BCzBN**. Furthermore, they are highly stable with decomposition temperature over 360 °C, which is important for stable and high brightness device operation (Fig. S7 and Table S1 in Supporting information) [24–26].

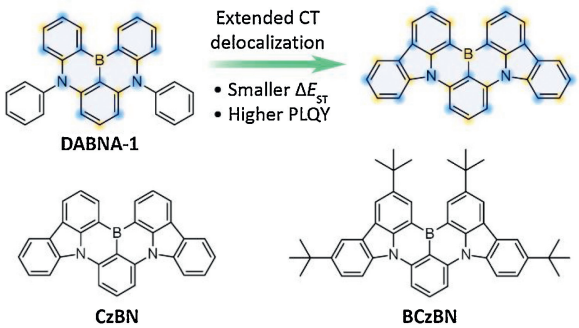

Fig. 1. Molecular design of solution-processible MR-molecules and structures of **CzBN** and **BCzBN**.

The ultraviolet-visible (UV–vis) absorption and PL spectra of **CzBN** and **BCzBN** were measured to investigate their photophysical properties (Figs. 2a and b and Table S1 in Supporting information) [27]. In dilute dichloromethane (DCM) solution, the two emitters exhibit dominative absorption bands at around 470 nm and narrow emission bands at 479 and 497 nm with FWHM of 30 and 28 nm, respectively. This should be a typical feature of MR molecules [12]. The small Stokes shifts (< 30 nm) are due to their rigid molecular structures [28]. In the neat film, **CzBN** exhibits a weak emission band at 502 nm and an additional broad emission band at 570 nm, where the first band at 502 nm should be the single molecular emission and that at 570 nm is attributed to the excimer emission owing to the nearly planar configuration for heavy aggregation [29,30]. The introduction of *tert*-butyls in **BCzBN** suppresses the aggregation in neat film, resulting in much enhanced single molecular emission at 517 nm that is comparable to the excimer emission around 571 nm. Dilute solutions of **CzBN** and **BCzBN** exhibit bright sky-blue and bluish-green emission in air with PLQYs of 87% and 86%, respectively (inset of Fig. 2c). The excimer induced emission around 570 nm was confirmed by doping **CzBN** and **BCzBN** into commonly used host material of 1,3-bis(9*H*-carbazol-9-yl)benzene (mCP). The doped films display similar

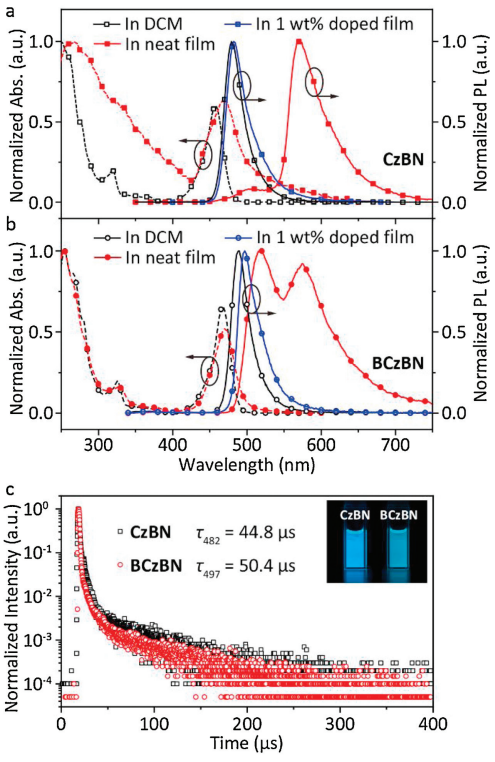

Fig. 2. Normalized absorption spectra (dash line) and emission spectra (solid line) of (a) **CzBN** and (b) **BCzBN** in DCM solution (black), neat film (red) and doped film in mCP (blue). (c) Delayed fluorescence decay curves of **CzBN** (black) and **BCzBN** (red) at 482 and 497 nm, respectively. Inset: photographs of diluted toluene solutions of **CzBN** and **BCzBN** excited by 365 nm UV light.

emission spectra to those in solution with also very small FWHM about 32 nm [31].

The phosphorescent spectra of **CzBN** and **BCzBN** were obtained at 77 K with a delay time of 30 ms (Fig. S8 in Supporting information) [32]. From the respective fluorescence and phosphorescence peaks at 478 and 502 nm, the ΔE_{ST} of 0.12 eV is identified for **CzBN**. Similarly, ΔE_{ST} of **BCzBN** is determined to be 0.11 eV on the basis of fluorescence and phosphorescence peaks at 498 and 520 nm. These ΔE_{ST}s are much smaller than the TADF criterion of 0.37 eV, suggesting that the two designed molecules are typical TADF emitters [33]. Their TADF feature was further confirmed by the time-resolved PL decays. Both short-lived prompt and long-lived delayed fluorescence components at room temperature were observed, exhibiting lifetimes of 7.0 and 8.4 ns (Fig. S9 in Supporting information) and 44.8 and 50.4 μs, respectively (Fig. 2c). It should be noted that both **CzBN** and **BCzBN** have smaller ΔE_{ST} than **DABNA-1** and their delayed fluorescence lifetimes are much shorter than 93.7 μs of **DABNA-1**, suggesting that both RISC and radiative decay processes of the fused MR molecules are more efficient than the original MR compound. These findings are in consistent with the kinetic rate constants of the photoluminescence (Table S2 in Supporting information), exhibiting accelerated prompt fluorescence (k_{PF}), intersystem crossing (k_{ISC}) and RISC (k_{RISC}) of **CzBN** and **BCzBN**.

To further clarify the MR and TADF characteristics of **CzBN** and **BCzBN**, density functional theory (DFT) and time-dependent DFT (TD-DFT) theoretical calculations were performed [34]. As shown in Fig. 3, **CzBN** and **BCzBN** exhibit atomically separated frontier molecular orbital (FMO) distributions similar to **DABNA-1**, where HOMOs distribute mainly on nitrogen atoms and carbon atoms at their *meta*-positions, and LUMOs locate primarily on boron atoms and carbon atoms at their *meta*-positions, except for the more extended distribution of FMOs and charge transfer (CT) delocalization areas due to their fused molecular structures. These typical MR-TADF molecule-featured FMO distributions are well in line with the electron density difference (EDD) and CT amount (q) analyses [14,35]. Their atomically alternative distributions of EDD show clearly the MR effects and extend to the phenyls far from boron atom, which is quite different to that of **DABNA-1**. Meanwhile, CT

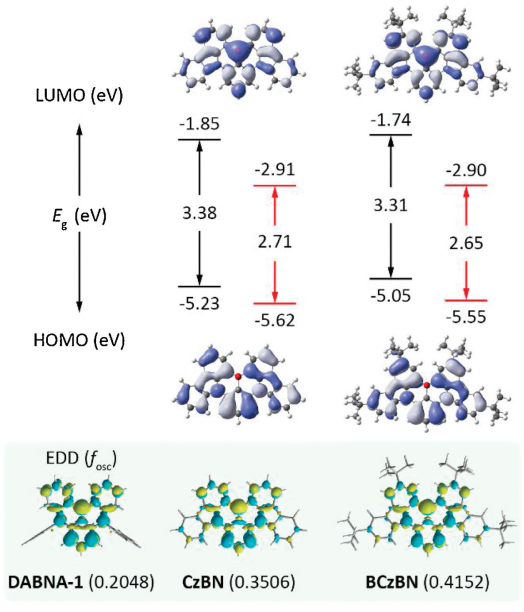

Fig. 3. HOMO and LUMO distributions and theoretical (black) and experimental (red) energy levels of **CzBN** and **BCzBN**, as well as EDD distributions and oscillator strength (f_{osc}) of **DABNA-1**, **CzBN** and **BCzBN**.

amounts of **CzBN** and **BCzBN** are 0.725 and 0.723 e, which are larger than that of **DABNA-1** (0.697 e), indicating the enhanced MR effects in these fused MR molecules (Tables S3–S5 in Supporting information). Therefore, not only reduced ΔE_{ST}, but also red-shifted emission are resulted with increased f_{osc} from 0.2048 for **DABNA-1** to 0.3506 and 0.4152 for **CzBN** and **BCzBN**, respectively. The highest f_{osc} of **BCzBN** should be due to both increased molecular rigidity and enhanced MR effect by introducing *tert*-butyl substitutes at *para*-positions of nitrogen atoms to strengthen the electron-donating ability of N atoms [36]. Moreover, the introduction of four electro-donating *tert*-butyl substitutes also raises the HOMO energy level for better hole injection and transport, which was confirmed by both the DFT calculations and cyclic voltammetry (CV) measurements (Fig. S10 in Supporting information) [37]. The high-lying HOMO around -5.5 eV and low-lying LUMO about -2.9 eV are highly attractive for hole and electron injection and transport, making it convenient in selecting host materials and other functional layers to fabricate TADF OLED devices.

In light of the highly soluble MR-TADF molecules of **BCzBN** with favorable FMO energy levels, we fabricated the solution-processed MR-OLEDs with the structure of ITO/PEDOT:PSS (40 nm)/emitting layer (EML, 50 nm)/DPEPO (10 nm)/TmPyPB (35 nm)/Liq (1 nm)/Al, where PEDOT:PSS (poly(3,4-ethylenedioxythiophene): poly(styrenesulfonic acid) and Liq (8-hydroxyquinolinolatolithium) act as hole- and electron-injection layers, DPEPO (bis(2-(diphenylphosphino) phenyl)ether oxide) serves as hole-blocking layer, TmPyPB (1,3,5-tri(m-pyrid-3-yl-phenyl)benzene) is electron-transporting layer (Figs. 4a and b) [38]. 10-(4-((4-(9*H*-Carbazol-9-yl)phenyl) sulfonyl)phenyl)-9,9-dimethyl-910-dihydroacridine (CzAcSF) is selected as the host materials in the EML with 2 wt%, 5 wt%, 10 wt% **CzBN** and **BCzBN** [39]. Indeed, very sharp electroluminescence (EL) spectra with small FWHM from 32 nm to 42 nm similar to the PL spectra were observed at different doping concentrations of MR-TADF emitters, indicating clearly the successful fabrication of solution-processed MR-OLEDs. The enlarged FWHM at increasing doping amount from 2 wt% to 10 wt% could be due to the enhanced guest aggregation at high concentrations. Impressively, the maximum current efficiency (CE), power efficiency (PE) and EQE of the sky-blue OLEDs based on **CzBN** reach 24.3 cd/A, 15.9 lm/W, and 14.7%, respectively, at the optimized doping concentration of 2 wt% (Table 1, and Figs. 4c and d). The much higher EQEs than the upper-limit (5%) of the conventional fluorescent OLEDs give the direct evidence that triplet excitons were harvested for EL through TADF mechanism. More excitingly, when **BCzBN** was employed as the emitter, improved device performances with CE of 31.1 cd/A, PE of 19.5 lm/W and EQE of 16.3% were achieved in the efficient bluish-green MR-OLEDs at a doping concentration of 2 wt% (Figs. 4e and f). These device performances are among the best results of solution-processed TADF OLEDs (Table S6 and Scheme S2 in Supporting information) [40].

In summary, a new design strategy for the solution-processible MR-TADF molecules was proposed by extending the CT delocalization of the MR backbone using both conjugated moieties and *tert*-butyl substituents. Two MR-TADF emitters with sky-blue and bluish-green emission were facilely prepared in two steps. It was found that the extension of π-conjugation and the introduction of electron-donating moieties at N-resonance positions to enhance the MR effect can narrow the bandgap and bathochromic-shift the emission spectra for small ΔE_{ST}, increased PLQY and good solubility. Unprecedentedly, the first solution-processed MR-TADF OLEDs exhibit the maximum CEs of 31.1 and 24.3 cd/A, PEs of 19.5 and 15.9 lm/W and EQEs of 16.3 and 14.7% for **BCzBN** and **CzBN**-based devices, respectively. These device performances are even better than the vacuum-deposited OLEDs based on **DABNA-1**, which may initiate the explorations of solution-processible MR materials and devices in the near future.

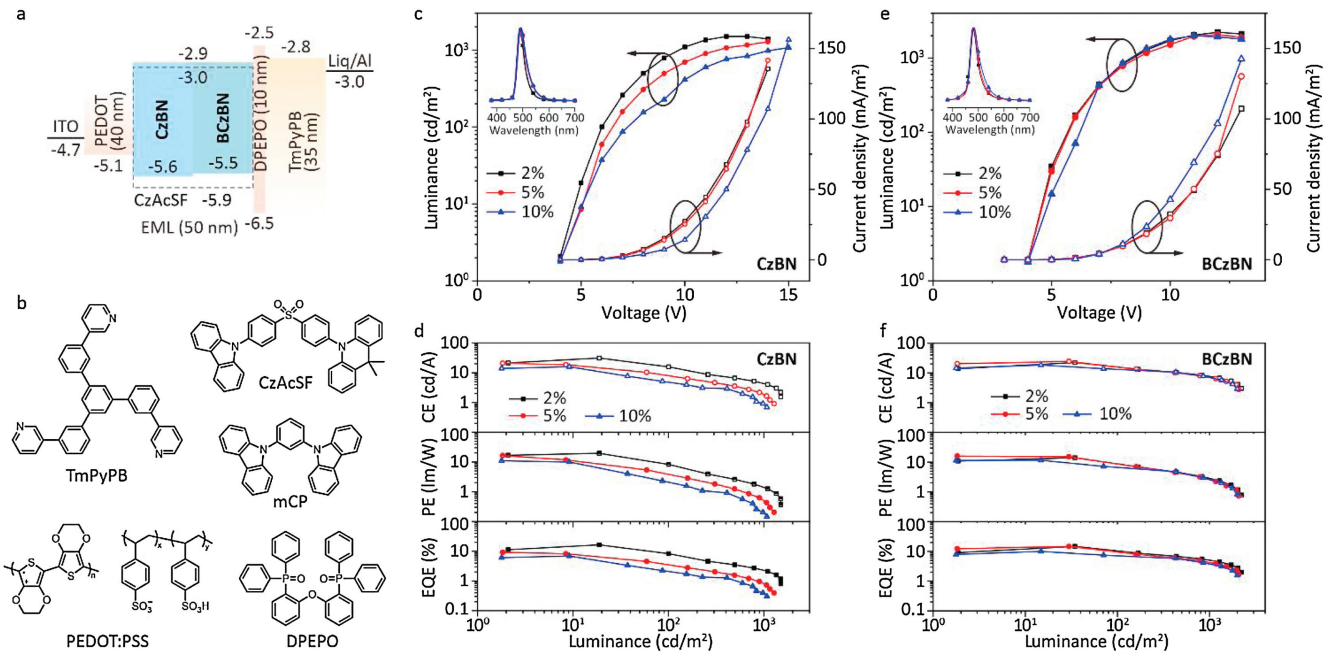

Fig. 4. (a) Structure and energy diagram of the solution-processed MR-TADF OLEDs. (b) Molecular structures of the adopted materials. Current density-voltage-luminance (*J-V*-L) curves (inset: EL spectra), current efficiency, power efficiency and external quantum efficiency curves of the devices at different doping concentration of (c, d) **CzBN** and (e, f) **BCzBN**.

Table 1
Device performance of the solution-processed MR-OLEDs.

Guest	Con. (%)	V_{on} (V)	Maximum efficiency			FWHM (nm)	λ_{EL} (nm)
			CE (cd/A)	PE (lm/W)	EQE (%)		
BCzBN	2	< 4	31.1	19.5	16.3	32	490
BCzBN	5	< 4	20.9	16.4	9.1	38	492
BCzBN	10	< 4	15.9	10.0	6.9	39	494
CzBN	2	< 4	22.3	14.0	14.7	35	480
CzBN	5	< 4	24.3	15.9	14.6	36	482
CzBN	10	< 4	18.4	11.5	10.0	42	484

Declaration of competing interest

The authors declare that they have no known competing financial interests or personal relationships that could have appeared to influence the work reported in this paper.

Acknowledgments

This study was supported by the National Natural Science Foundation of China (Nos. 21772095, 91833306, 51873159, 91956107, 61875090 and 21674049), 1311 Talents Program of Nanjing University of Posts and Telecommunications (Dingshan), the Six Talent Plan (No. 2016XCL050), the Priority Academic Program Development of Jiangsu Higher Education Institutions (PAPD, No. YX030003), China Postdoctoral Science Foundation (No. 2020M671460), Jiangsu Planned Projects for Postdoctoral Research Funds (No. 2020Z137), and Postgraduate Research & Practice Innovation Program of Jiangsu Province (No. 46030CX17761).

Appendix A. Supplementary data

Supplementary material related to this article can be found, in the online version, at doi:https://doi.org/10.1016/j.cclet.2020.10.022.

References

[1] Y. Liu, C. Li, Z. Ren, S. Yan, M.R. Bryce, Nat. Rev. Mater. 3 (2018) 18020.
[2] Z. Yang, Z. Mao, Z. Xie, et al., Chem. Soc. Rev. 46 (2017) 915–1016.
[3] Y. Tao, K. Yuan, T. Chen, et al., Adv. Mater. 26 (2014) 7931–7958.
[4] A. Endo, M. Ogasawara, A. Takahashi, et al., Adv. Mater. 21 (2009) 4802–4806.
[5] H. Uoyama, K. Goushi, K. Shizu, H. Nomura, C. Adachi, Nature 492 (2012) 234–238.
[6] T. Wu, M. Huang, C. Lin, et al., Nat. Photon. 12 (2018) 235–240.
[7] D.H. Ahn, S.W. Kim, H. Lee, et al., Nat. Photon. 13 (2019) 540–546.
[8] A. Endo, K. Sato, K. Yoshimura, et al., Appl. Phys. Lett. 98 (2011) 83302.
[9] Q. Zhang, B. Li, S. Huang, et al., Nat. Photon. 8 (2014) 326–332.
[10] T. Lin, T. Chatterjee, W. Tsai, et al., Adv. Mater. 28 (2016) 6976–6983.
[11] P.K. Samanta, D. Kim, V. Coropceanu, J. Brédas, J. Am. Chem. Soc. 139 (2017) 4042–4051.
[12] T. Hatakeyama, K. Shiren, K. Nakajima, et al., Adv. Mater. 28 (2016) 2777–2781.
[13] H. Hirai, K. Nakajima, S. Nakatsuka, et al., Angew. Chem. Int. Ed. 54 (2015) 13581–13585.
[14] A. Pershin, D. Hall, V. Lemaur, et al., Nat. Commun. 10 (2019) 597.
[15] Y. Gao, Q. Pan, L. Zhao, et al., Chem. Phys. Lett. 701 (2018) 98–102.
[16] Y. Kondo, K. Yoshiura, S. Kitera, et al., Nat. Photon. 13 (2019) 678–682.
[17] X. Liang, Z. Yan, H. Han, et al., Angew. Chem. Int. Ed. 57 (2018) 11316–11320.
[18] S. Nakatsuka, H. Gotoh, K. Kinoshita, N. Yasuda, T. Hatakeyama, Angew. Chem. Int. Ed. 56 (2017) 5087–5090.
[19] K. Matsui, S. Oda, K. Yoshiura, et al., J. Am. Chem. Soc. 140 (2018) 1195–1198.
[20] M. Hirai, N. Tanaka, M. Sakai, S. Yamaguchi, Chem. Rev. 119 (2019) 8291–8331.
[21] Y. Zhang, D. Zhang, J. Wei, et al., Angew. Chem. Int. Ed. 58 (2019) 16912–16917.
[22] Y. Xu, Z. Cheng, Z. Li, et al., Adv. Opt. Mater. 8 (2020) 1902142.
[23] S. Xu, H. Li, R. Chen, et al., Adv. Opt. Mater. 6 (2018) 1701105.
[24] J. Jin, Y. Tao, H. Jiang, et al., Adv. Sci. 5 (2018) 1800292.

[25] D. Zhou, D. Liu, X. Gong, et al., ACS Appl. Mater. Interfaces 11 (2019) 24339–24348.
[26] D. Zhou, C.H. Ryoo, D. Liu, et al., Adv. Opt. Mater. 8 (2020) 1901021.
[27] H. Li, Y. Tao, Y. Zhi, et al., Chem. Eng. J. 380 (2020) 122562.
[28] M. Irfan, J. Mahar, A. Saeed, K.D. Belfield, M. Siddiq, J. Chin. Chem. Soc. 65 (2018) 243–251.
[29] S. Xu, H. Li, Y. Tang, et al., Aust. J. Chem. 69 (2016) 419–422.
[30] D. Zhao, Q. Wu, Z. Cai, et al., Chem. Mater. 28 (2016) 1139–1146.
[31] X. Li, Y. Shi, K. Wang, et al., ACS Appl. Mater. Interfaces 11 (2019) 13472–13480.
[32] C. Duan, J. Li, C. Han, et al., Chem. Mater. 28 (2016) 5667–5679.
[33] R. Chen, Y. Tang, Y. Wan, et al., Sci. Rep. 7 (2017) 6225.
[34] L. Lin, J. Fan, L. Cai, C. Wang, Mol. Phys. 116 (2018) 19–28.
[35] S. Huang, Q. Zhang, Y. Shiota, et al., J. Chem. Theory Comput. 9 (2013) 3872–3877.
[36] D. Zhang, M. Cai, Y. Zhang, D. Zhang, L. Duan, Mater. Horiz. 3 (2016) 145–151.
[37] S. Tan, X. Wu, Y. Zheng, Y. Wang, Chin. Chem. Lett. 30 (2019) 1951–1954.
[38] X. Zheng, R. Huang, C. Zhong, et al., Adv. Sci. 7 (2020) 1902087.
[39] W. Song, I. Lee, J.Y. Lee, Adv. Mater. 27 (2015) 4358–4363.
[40] Y. Tang, G. Xie, X. Liang, Y. Zheng, C. Yang, J. Mater. Chem. C 8 (2020) 10831–10836.